Materials Transactions, Vol. 57, No. 12 (2016) pp. 2020 to 2025
Special Issue on Advances in Biomedical Materials Science and Technology

Cytocompatibility of Ti–6Al–7Nb through High-Pressure Torsion Processing

Peng Chen[1], Maki Ashida[1], Hisashi Doi[1], Yusuke Tsutsumi[1,2], Zenji Horita[3,4] and Takao Hanawa[1,*]

[1]*Department of Metallic Biomaterials, Institute of Biomaterials and Bioengineering, Tokyo Medical and Dental University, Tokyo 101–0062, Japan*
[2]*Graduate School of Engineering, The University of Tokyo, Tokyo 113–8656, Japan*
[3]*Department of Materials Science and Engineering, Kyushu University, Fukuoka 819–0395, Japan*
[4]*WPI, International Institute for Carbon-Neutral Energy Research (WPI-I2CNER), Kyushu University, Fukuoka 819–0395, Japan*

In this study, we evaluated the cytocompatibility of high-pressure torsion (HPT)-processed Ti-6Al-7Nb alloys. Grain size of titanium (Ti) alloys decreased from 5 μm (without HPT processing, HPT-0) to ~100 nm (at 2 GPa, HPT-2) or ~70 nm (at 6 GPa, HPT-6) through HPT processing. Cell adhesion, proliferation, and differentiation were evaluated with mouse preosteoblast (MC3T3-E1). A locomotion trend was presented by cells cultured on HPT-2 to compare with other specimens, while, an immobilization trend was presented by cells cultured on HPT-6 to compare with other specimens. *Akp2* (alkaline phosphatase 2) expression was higher in cells cultured on HPT-2 than that on HPT-0 and HPT-6, indicating enhanced osteogenic differentiation. Our results demonstrate that HPT-processed Ti-6Al-7Nb alloys offer good cytocompatibility. [doi:10.2320/matertrans.MI201515]

(Received May 30, 2016; Accepted October 5, 2016; Published November 7, 2016)

Keywords: *titanium alloys, high-pressure torsion, adhesion, osteogenic differentiation*

1. Introduction

Ti–6Al–7Nb alloy is an alternative metallic biomaterial for medical applications. It offers superior resistance to corrosion and low toxicity. However, as an α+β type Ti alloy, it has limited cold-formability due to high strength and low ductility. In a previous work[1)], we successfully employed high-pressure torsion (HPT) processing to improve the mechanical properties of the Ti–6Al–7Nb alloy. HPT increased tensile strength while maintaining the elongation. This was attained by decreasing grain size of the alloy from 5 μm to about 100 nm[1)]. However, the cytocompatibility of this HPT processed Ti alloy has not been assessed yet.

Grain refinement is thought to be an important role in the cytocompatibility of substrate[2–9)], such as cell attachment. It was reported that improved cell attachment was observed by a nano-grained Ti–29Nb–13Ta–4.6Zr alloy, on which osteoblast displayed larger number of filopodia protrusions compared with alloy without grain refinement[2)]. Expression of fibronectin, vinculin (focal adhesions), and actin (cytoskeleton) were also found to be affected by grain refinement[3–5)]. One potential reason for this phenomenon would be the grain refinement increases the grain boundaries, interfaces, and high dislocation density, which result a high wettability leading to a larger number of lamellipodia structures around the cells and hereby an improved cell attachment[2)].

In addition, grain size could also have effect on cell proliferation and differentiation. A significantly higher proliferation rate was reported by cells incubated on grain-refined Ti[4)] or Ti–6Al–4V alloy[7)] compared with those growing on a non-refined alloy. Cell differentiation was also found to respond to grain refinement[8,9)], possibly as a result of changes in surface chemical composition[10,11)], such as alterations in surface hydrophilicity and protein adsorption[12,13)], changes in corrosion properties[14)], and also a more open lattice in the position of high-angle boundaries[2,5,15)].

In the present study, we addressed the cytocompatibility of Ti–6Al–7Nb alloy processed with HPT. The cell adhesion, proliferation and osteogenic differentiation were evaluated with mouse preosteoblast (MC3T3-E1). The information offered by work would be important for the HPT processed Ti–6Al–7Nb alloys to be applied for potential biomedical using.

2. Experimental Procedure

2.1 Specimen preparation

A commercial Ti–6Al–7Nb alloy (ASTM F1295) was purchased from the Nilaco Corporation (Tokyo, Japan). The specimens with and without HPT processing were prepared as described previously[1)]. Briefly, a Ti–6Al–7Nb alloy rod with a diameter of 10 mm was prepared and cut into 0.8-mm-thick slices. HPT conditions were as previously described: pressure, 2 or 6 GPa; rotation speed, 1 rpm; revolution number, 5; and room temperature. All specimens were polished mechanically on both sides with SiC paper and mirror-finished on one side with a 0.04-μm colloidal silica suspension (Struers, Tokyo, Japan). Subsequently, they were ultrasonically rinsed in acetone and ethanol, dried with a stream of nitrogen gas (99.9%), and finally kept in an auto-dry desiccator until use. Specimens were designated according to the type of HPT processing, thus HPT-0, HPT-2, and HPT-6 indicated lack of treatment, 2 GPa, and 6 GPa, respectively. In addition, grain size of specimens with or without HPT processing was measured by dark-field transmission electron microscopy.

2.2 Surface characterization

Specimen surface composition and chemical states were characterized by X-ray photoelectron spectroscopy (XPS, JPS–9010MC; JEOL, Tokyo, Japan). A monochromatized Mg Kα line (1253.6 eV) was used as X-ray source and the take-off angle of photoelectrons was 90° with respect to the detection surface. All binding energies were relative to the

*Corresponding author, E-mail: Hanawa.met@tmd.ac.jp

Fermi level. The C 1s peak at 285.0 eV originating from hydrocarbon contamination was used to calibrate the binding energies of peaks in the XPS spectra. In order to estimate integrated peak intensities, the background was subtracted from the measured spectra according to Shirley's method. Energy values have been reported elsewhere[16]. The composition and thickness of the surface oxide film were calculated as previously described[17,18]. Empirical data[19–22] on relative photoionization cross-sections, σ_{ij}/σ_{O1s} (Table 1), were used for quantification, where σ_{ij}/σ_{O1s} represented a level j electron of an element i relative to that of O 1s electrons. Relative concentrations of elements and thickness of the surface oxide film were calculated, except for carbon, which was considered a contaminant.

2.3 Cell culture and induction of osteogenic differentiation

As described previously[23,24], a mouse preosteoblast cell line (MC3T3–E1, RIKEN BioResource Center, Ibaraki, Japan) was maintained in alpha modified Eagle's minimum essential medium (α-MEM; Gibco, Carlsbad, CA, USA) supplemented with 10% fetal bovine serum (Gibco) and an antibiotic/antimycotic (Gibco). Cells were seeded onto sterilized specimens at an approximate density of 5000 cells·cm^{-2}. Tissue-culture-treated polystyrene dishes (TCPS) were used as controls for evaluation of gene expression and cell proliferation. Cells were incubated at 37°C in a humidified atmosphere of 5% CO_2 in air.

To induce osteogenic differentiation, cells were grown to 100% confluence and shifted to induction medium consisting of culture medium supplemented with 2 mM β-glycerophosphate (Calbiochem, Darmstadt, Germany) and 50 mg·mL^{-1} L-ascorbic acid (Wako Pure Chemical Industries, Osaka, Japan). Induction medium was changed every 3 days. All specimens were sterilized in 70% ethanol for 20 min and subsequently thoroughly rinsed with deionized water before cell seeding.

2.4 Attached cell counts

The number of cells on each specimen was quantified using Cell Counting Kit-8 (Dojindo Laboratories, Kumamoto, Japan) according to manufacturer instructions and described in our previous report[23]. Sample absorbance at 450 nm was measured using a ChroMate® microplate reader (Awareness Technology, Inc., Palm City, FL, USA).

2.5 Immunocytochemistry and imaging

The morphology of cells cultured on Ti–6Al–7Nb alloys with or without HPT processing was visualized by immunofluorescence staining. After incubation for 3 h, cells were fixed in 4% paraformaldehyde (Taab Laboratory Equipment Ltd., Reading, UK) and blocked in 10% goat serum (Sigma-Aldrich Corp., St. Louis, MO, USA). Cytoskeletal actin was visualized by staining with rhodamine phalloidin (Cytoskeleton Inc., Denver, CO, USA) and nuclei were counterstained with 4',6-diamidino-2-phenylindole (DAPI, Invitrogen, Carlsbad, CA, USA). Adhesion plaques were visualized by immunocytochemical labeling of vinculin with a monoclonal anti-vinculin antibody (Sigma-Aldrich), followed by Alexa Fluor 488-conjugated goat anti-mouse IgG (Invitrogen). Digital images were acquired using an IX71 microscope with DP70 charge-coupled device camera (Olympus Optical Co. Ltd., Tokyo, Japan).

Table 1 Photoionization cross sections of level j of element i relative to that of the O1s, σ_{ij}/σ_{O1s}.

Level	Photoionization cross sections		
	Ti $2p_{3/2}$	Nb 3d	Al 2p
σ_{ij}/σ_{O1s}	1.28	2.98	0.19
Reference	19	21	22

2.6 Real-time RT-PCR

Quantitative real-time RT-PCR was used to measure expression of selected target genes. *Vcl* (vinculin) was selected as a reporter of cell attachment, while *Runx2* (runt-related transcription factor 2), *Col1α1* (procollagen, type I), and *Akp2* (alkaline phosphatase 2) were selected as markers of osteogenic differentiation. The procedure was described previously elsewhere[23]. Briefly, total RNA was extracted with an RNeasy Kit (Qiagen GmbH, Hilden, Germany), in accordance with manufacturer instructions. RNA (2 μg) was reverse-transcribed into complementary DNA (cDNA) using a random hexamer primer and the PrimeScript II 1st Strand cDNA Synthesis System (Takara Biotechnology Co. Ltd., Dalian, China), in accordance with manufacturer instructions. The reaction mixture contained 10 μL SYBR Premix Ex Taq II (Takara Biotechnology Co., Ltd.), 10 pmol each of forward and reverse primers, 2 μL cDNA, and distilled water to a final volume of 20 μL. The reaction was carried out on a LightCycler 480 (Roche Diagnostics GmbH, Mannheim, Germany). The housekeeping *Gapdh* gene encoding glyceraldehyde 3-phosphate dehydrogenase was used for normalization. The primers used in this study were purchased from Takara Bio Co., Ltd. (Table 2).

2.7 Statistical analysis

All values represent at least three independent tests ($n \geq 3$) and are shown as mean ± standard deviation. Gene expression in osteogenic differentiation experiments was analyzed by Student's t-test for each two groups using MS Excel software (Microsoft Corp., Redmond, WA, USA). Attached cell counts and vinculin gene expression were analyzed by one-way analysis of variance followed by a Student-Newman-Keuls test for multiple comparisons using SPSS Statistics v.22 software (SPSS, Chicago, IL, USA). $P < 0.05$ was considered statistically significant.

3. Results and Discussion

3.1 Surface chemical composition

The XPS spectrum of O 1s (Fig. 1(a)) consisted of three chemical states[20]: oxide (O^{2-}), hydroxide or hydroxyl groups (OH^-), or hydrated and/or adsorbed water (H_2O). Regions corresponding to these chemical states of oxygen and the relative amounts of O^{2-}, OH^-, H_2O, and $[OH^-]/[O^{2-}]$ value were calculated to determine the chemical state of the surface oxide. There were thin surface oxide films on all specimens. Compared with HPT-0, slightly thicker surface oxide films

Table 2 Description of target genes and sequence of oligonucleotide primers for real-time RT-PCR.

Target gene	Description	Sequence of oligonucleotide primers
Vcl	*M. musculus* cytoskeletal protein associated with cell-cell and cell-matrix junctions, where it is thought to function as one of several interacting proteins involved in anchoring F-actin to the membrane.	Forward: TCTCGCACCTGGTGATTATGC Reverse: TGAACAGTCTCTTTTCCAACCC
Runx2	*M. musculus* runt-related transcription factor 2 is a key transcription factor associated with osteoblast differentiation.	Forward: CACTGGCGGTGCAACAAGA Reverse: TTTCATAACAGCGGAGGCATTTC
Col1α1	*M. musculus* procollagen, type I, alpha 1, encodes the major component of fibrillar collagen found in most connective tissues, including cartilage, which is used as a marker for osteoblast differentiation.	Forward: TGCTGGACGTCCTGGTGAAG Reverse: ACGTTGTCCAGCAATACCCTGAG
Akp2	*M. musculus* alkaline phosphatase 2 encodes a membrane-bound enzyme that is used as a marker for maturity of osteoblast.	Forward: TGCCTACTTGTGTGGCGTGAA Reverse: TCACCCGAGTGGTAGTCACAATG
Gapdh	*M. musculus* glyceraldehyde 3-phosphate dehydrogenase is a housekeeping gene.	Forward: TGTGTCCGTCGTGGATCTGA Reverse: TTGCTGTTGAAGTCGCAGGAG

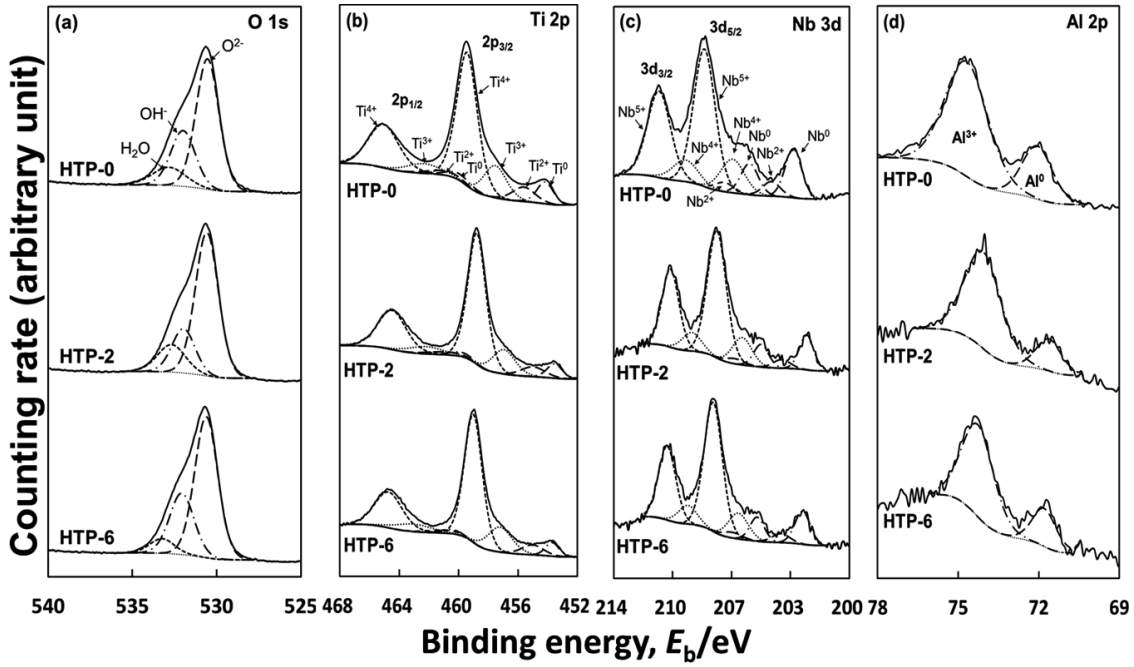

Fig. 1 O 1s, Ti 2p, Nb 3d, and Al 2p electron energy regions of XPS spectra from Ti-6Al-7Nb alloys with or without HPT processing.

Table 3 Relative concentration of elements, $[Ti^{4+}]/[Ti^{2+}+Ti^{3+}+Ti^{4+}]$ ratio, $[OH^-]/[O^{2-}]$ ratio, and thickness of surface films on Ti-6Al-7Nb alloys with or without HPT processing.

Detected specimens	Relative concentrations (at%)				$[Ti^{4+}]/[Ti^{2+}+Ti^{3+}+Ti^{4+}]$	$[OH^-]/[O^{2-}]$	Binding energy of Ti $2p_{3/2}$ (Eb/eV)	Thickness of oxide film (nm)
	Ti	Al	Nb	O				
HPT-0	24.9	0.2	0.7	74.2	0.83	0.16	458.57	6.4
HTP-2	22.4	0.2	0.8	76.6	0.88	0.26	459.14	7.0
HTP-6	23.4	0.2	0.7	75.8	0.87	0.28	459.42	6.8

were observed on Ti alloys after HPT processing (HPT-2 and HPT-6) (Table 3). The spectra of metallic elements, Ti 2p (Fig. 1(b)), Nb 3d (Fig. 1(c)), and Al 2p (Fig. 1(d)), consisted of two chemical states: oxide (positive valence, M^{n+}, from surface passive oxide film) and pure metal (zero valence, M^0, from the alloy substrate under surface passive oxide film). After HPT processing, the $[Ti^{4+}]/[Ti^{2+}+Ti^{3+}+Ti^{4+}]$ ratio increased and the binding energy of Ti $2p_{3/2}$ shifted to a higher energy state (Table 3), indicating that specimens with HPT processing had more surface oxidation. This phenomenon could be explained by the refinement of grain size of the alloys. We have previously shown that after HPT processing grain size of the α phase decreased from 5 μm in HPT-0 to about 100 nm or 70 nm in HPT-2 and HPT-6, respectively[1], which could result in enhanced surface oxidation. In general, no significant change in surface chemical composition of specimens was observed by XPS.

3.2 Cell adhesion

The number of cells attached to Ti–6Al–7Nb alloys with or without HPT processing was similar 3 h after cell seeding (Fig. 2). This indicated that HPT processing did not affect the number of attached cells within the first 3 h of incubation.

Cell extension was visualized by immunofluorescence staining (Fig. 3 and Fig. 4), after 3 h of incubation. Depending on the specimen, we detected differences in the shape of cells (Fig. 3). Spreading shapes were most common on HPT-6, round shapes dominant on HPT-2, and both shapes were observed on HPT-0. We monitored the cells at a higher magnification to assess the location and shape of adhesion plaques by vinculin staining (Fig. 4). Cells cultivated on HPT-6 and to a lesser extent on HPT-0 presented a fibrous structure at the margin of the pseudopodia, whereas cells growing on HPT-2 and less markedly on HPT-0 displayed a pointed distribution

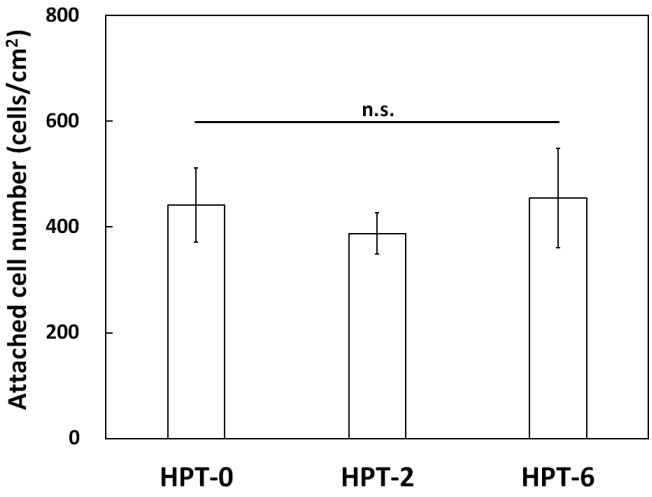

Fig. 2 Number of MC3T3-E1 cells attached to Ti-6Al-7Nb alloys with or without HPT processing after 3 h of incubation. n.s., non-significant.

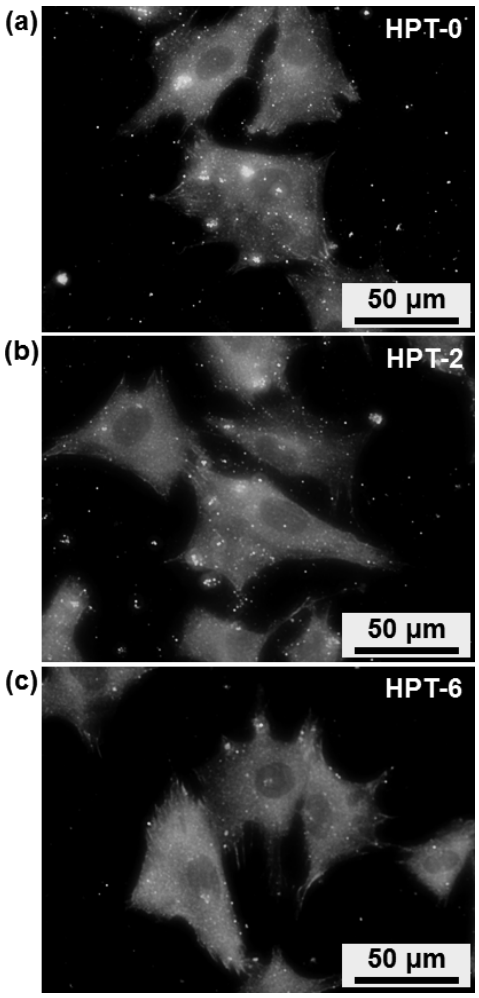

Fig. 4 Fluorescence microscopy of adhesion plaque distribution in MC3T3-E1 cells attached to Ti-6Al-7Nb alloys with or without HPT processing after 3 h of incubation. Nuclei (blue) and adhesion plaques (vinculin, green) were visualized.

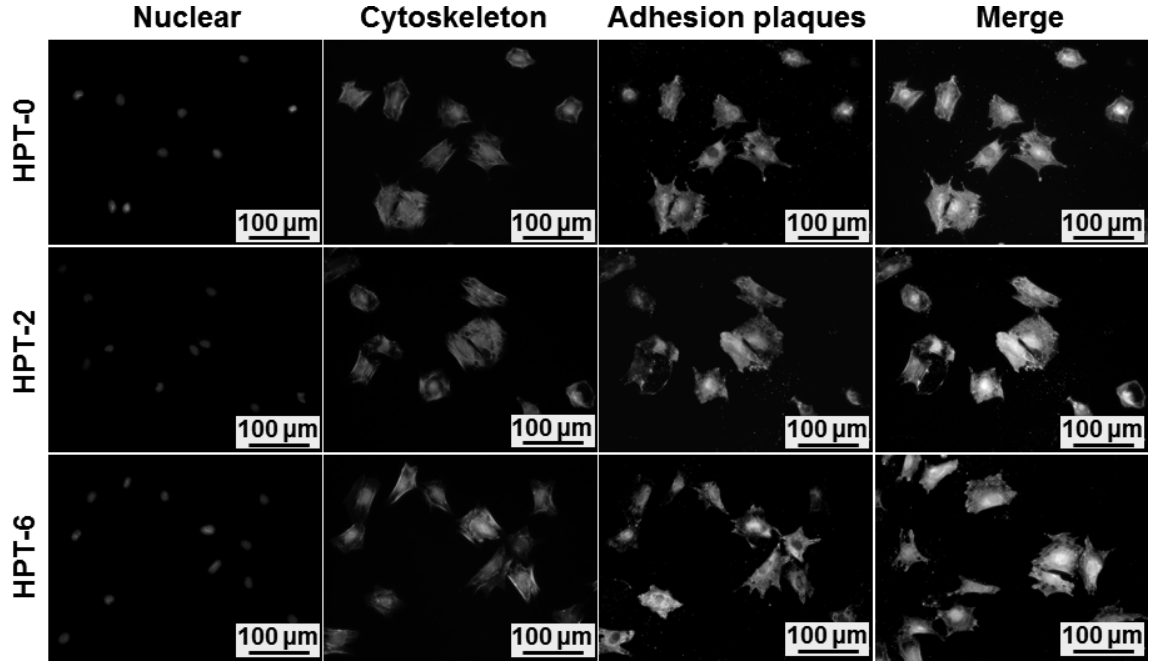

Fig. 3 Fluorescence microscopy of MC3T3-E1 cells attached to Ti-6Al-7Nb alloys with or without HPT processing after 3 h of incubation. Nuclei (blue), cytoskeleton (F-actin, red), and adhesion plaques (vinculin, green) were visualized.

of adhesion plaques. Considering vinculin's role in cell adhesion[25,26], the shape of cells cultured on HPT-6 indicated a stronger cell immobilization trend, whereas those on HPT-2 presented a stronger cell locomotion trend compared with other specimens. Cells cultured on HPT-0 showed an intermediate pattern.

Cells cultured on TCPS had higher *Vcl* expression level than those growing on Ti–6Al–7Nb substrates after incubation for 3 h (Fig. 5). Expression of *Vcl* in cells cultured on Ti–6Al–7Nb alloys processed with HPT was lower than in the absence of HPT (HPT-0 > HPT-6 > HPT-2). This result appears to differ from previously reported vinculin protein expression data[3–5]. Considering the good cytocompatibility of Ti–6Al–7Nb alloys, refinement of grain size may not significantly improve cell adhesion. In addition, the resulting protein levels may not correlate with gene expression. Figure 4 shows strong fluorescence intensity in cells cultured on HPT-0 and HPT-2. It is possible that *Vcl* expression peaked before the 3 h incubation was complete and thus was overlooked.

3.3 Cell proliferation

Cell proliferation was evaluated for 5 days. The number of cells attached increased along with the incubation time for all specimens (Fig. 6). After 1 day, there was no significant difference in cell attachment among Ti–6Al–7Nb alloys with or without HPT processing. However, on the third day more cells were harvested by HPT-0 than that by HPT-2 or HPT-6. After 5 days, the number of cells cultured on all Ti–6Al–7Nb alloys was similar and was larger than that seen on TCPS, confirming previous reports[4].

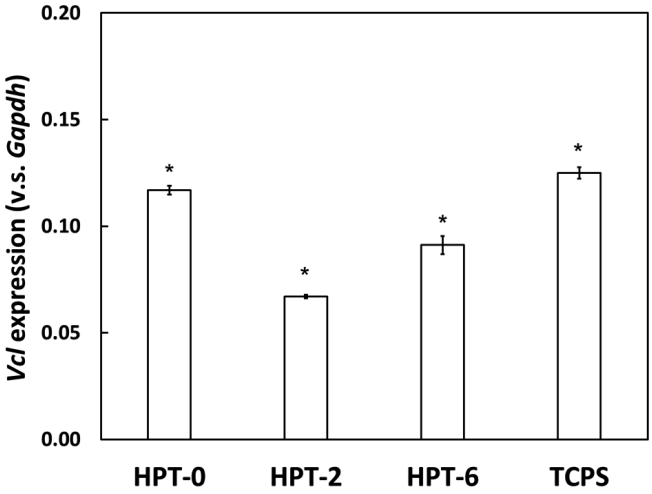

Fig. 5 *Vcl* expression level in MC3T3-E1 cells cultured on Ti-6Al-7Nb alloys with or without HPT processing and TCPS after 3 h of incubation. Values correspond to the mean ± standard deviation (n ≥ 3). * *P* value < 0.05 was deemed statistically significant.

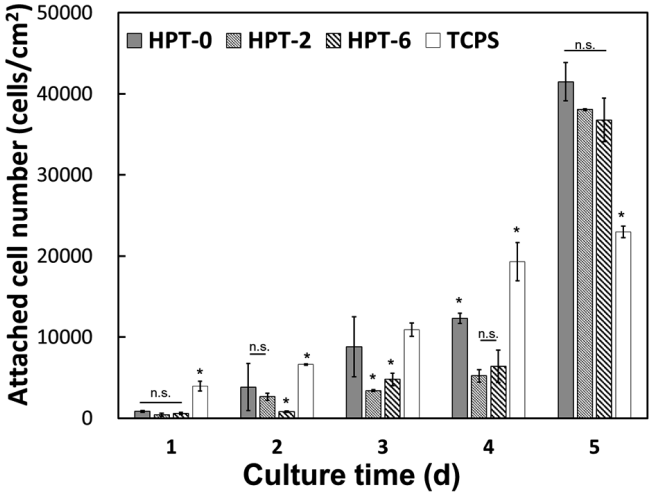

Fig. 6 Proliferation of MC3T3-E1 cells on Ti-6Al-7Nb alloys with or without HPT processing and TCPS after 5 days. Values correspond to the mean ± standard deviation (n ≥ 3). * *P* value < 0.05 was deemed statistically significant. n.s., non-significant.

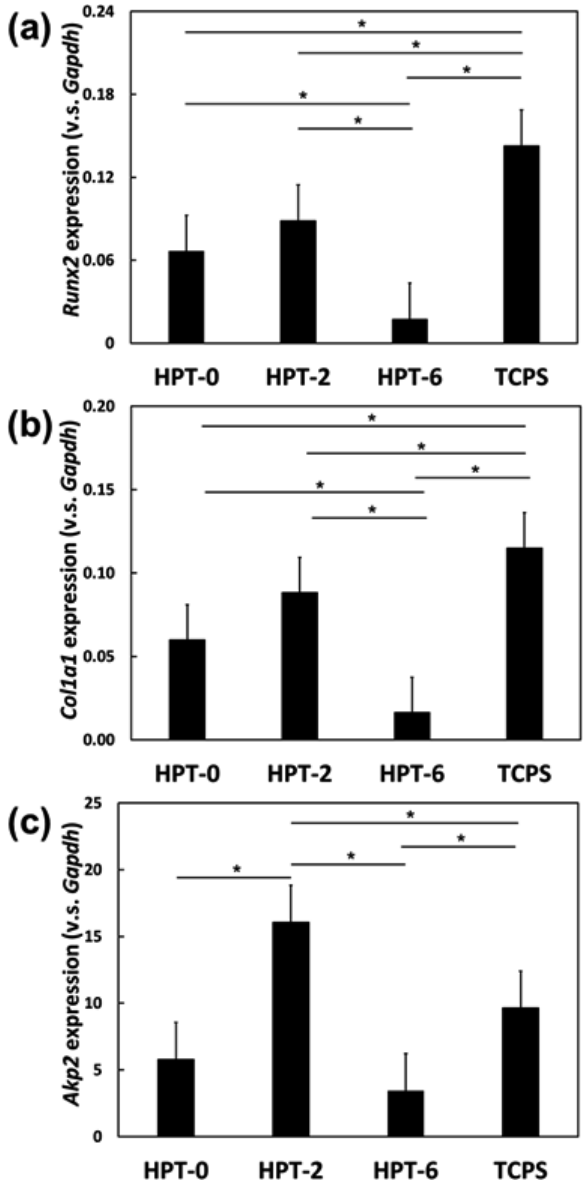

Fig. 7 Histograms of target mRNA expression levels in MC3T3-E1 cells cultured on Ti-6Al-7Nb alloys with or without HPT processing and TCPS after 7 days of induction The expression of (a) *Runx2*, (b) *Col1α1*, and (c) *Akp2* was detected by real-time RT-PCR. Values correspond to the mean ± standard deviation (n ≥ 3). * *P* value < 0.05 was deemed statistically significant.

3.4 Osteogenic differentiation

Osteogenic differentiation was induced in preosteoblasts and expression of three target genes was investigated after 7 days. The highest expression of *Runx2* and *Col1α1* was obtained in cells cultured on TCPS (Fig. 7), whereas *Akp2* was highest in those cultured on HPT-2, suggesting possible osteoblast maturation. Cells cultured on HPT-6 consistently yielded the lowest expression levels for all genes, while HPT-0 showed intermediate expression levels. These results indicated that HPT-processed Ti–6Al–7Nb alloys could have an effect on cell differentiation and ~100-nm grain size HPT-2 could promote the maturation of MC3T3-E1.

4. Conclusions

HPT processing decreased the grain size of Ti alloys from a micrometer to a nanometer scale, leading to a slightly larger surface oxidization. For cell attachment, a locomotion trend was presented by cells cultured on HPT-2 to compare with other specimens, while, an immobilization trend was presented by cells cultured on HPT-6 to compare with other specimens. A larger number of proliferated cells were obtained by Ti alloys with and without HPT processing than that on TCPS after 5 days of cultivation. In addition, a higher *Akp2* expression level was observed in cells cultured on HPT-2 after 7 days of induction, indicating stimulated osteoblast maturation. Our results indicated that HPT-processed Ti–6Al–7Nb alloys could have similar good cytocompatibility as Ti–6Al–7Nb does, although there were some differences in cell adhesion, proliferation, and osteogenic differentiation. In summary, HPT-processed Ti-6Al-7Nb alloy has good cytocompatibility and could be a potential candidate for biomedical applications.

Acknowledgments

This work was partially supported by the Japan Science Promotion Society (Grant-in-Aid for Young Scientists B, No. 15K20473) and the Light Metal Educational Foundation, Inc. The HPT process was carried out in the International Research Center on Giant Straining for Advanced Materials (IRC-GSAM) at Kyushu University.

REFERENCES

1) M. Ashida, P. Chen, H. Doi, Y. Tsutsumi, T. Hanawa and Z. Horita: Mater. Sci. Eng. A **640** (2015) 449–453.
2) H. Yilmazer, M. Şen, M. Niinomi, M. Nakai, H.H. Liu, K. Cho, Y. Todaka, H. Shiku and T. Matsue: RSC Adv. **6** (2016) 7426–7430.
3) S. Bagherifard, D.J. Hickey, A.C. de Luca, V.N. Malheiro, A.E. Markaki, M. Guagliano and T.J. Webster: Biomaterials **73** (2015) 185–197.
4) S. Faghihi, F. Azari, A.P. Zhilyaev, J.A. Szpunar, H. Vali and M. Tabrizian: Biomaterials **28** (2007) 3887–3895.
5) R.D.K. Misra, W.W. Thein-Han, T.C. Pesacreta, M.C. Somani and L.P. Karjalainen: Acta Biomater. **6** (2010) 3339–3348.
6) S. Faghihi, H. Vali and M. Tabrizian: Int. J. Mod. Phys. B **22** (2008) 3069–3081.
7) P. Han, W.P. Ji, C.L. Zhao, X.N. Zhang and Y. Jiang: Chinese Med. J. **124** (2011) 273–279.
8) C.H. Park, C.S. Lee, Y.J. Kim, J.H. Jang, J.Y. Suh and J.W. Park: Clin. Oral Implants Res. **22** (2011) 735–742.
9) C. Nune and R.D.K. Misra: Mater. Technol. **30** (2015) 76–85.
10) M. Hoseini, P. Bocher, A. Shahryari, F. Azari, J.A. Szpunar and H. Vali: J. Biomed. Mater. Res. A **102** (2014) 3631–3638.
11) D.N.A. Shri, K. Tsuchiya and A. Yarnamoto: Mater. Sci. Eng. C **43** (2014) 411–417.
12) C. Nune, R.D.K. Misra, M.C. Somani and L.P. Karjalainen: J. Biomed. Mater. Res. A **102** (2014) 1663–1676.
13) R.D.K. Misra, C. Nune, T.C. Pesacreta, M.C. Somani and L.P. Karjalainen: J. Biomed. Mater. Res. A **101** (2013) 1–12.
14) F.L. Nie, Y.F. Zheng, Y. Cheng, S.C. Wei and R.Z. Valiev: Mater. Lett. **64** (2010) 983–986.
15) Y. Mine, T. Tsumagari and Z. Horita: Scr. Mater. **63** (2010) 552–555.
16) K. Asami: J. Electron Spectrosc. Relat. Phenom. **9** (1976) 469–478.
17) K. Asami and K. Hashimoto: Corros. Sci. **24** (1984) 83–97.
18) K. Asami, K. Hashimoto and S. Shimodaira: Corros. Sci. **17** (1977) 713–723.
19) K. Asami, S.C. Chen, H. Habazaki, A. Kawashima and K. Hashimoto: Corros. Sci. **31** (1990) 727–732.
20) K. Asami, S.C. Chen, H. Habazaki and K. Hashimoto: Corros. Sci. **35** (1993) 43–49.
21) X.Y. Li, E. Akiyama, H. Habazaki, A. Kawashima, K. Asami and K. Hashimoto: Corros. Sci. **40** (1998) 821–838.
22) H. Yoshioka, H. Habazaki, A. Kawashima, K. Asami and K. Hashimoto: Corros. Sci. **32** (1991) 313–325.
23) P. Chen, A. Nagai, Y. Tsutsumi, M. Ashida, H. Doi and T. Hanawa: J. Biomed. Mater. Res. A **104** (2016) 639–651.
24) T. Umezawa, P. Chen, Y. Tsutsumi, H. Doi, M. Ashida, S. Suzuki, K. Moriyama and T. Hanawa: Dent. Mater. J. **34** (2015) 713–718.
25) J.L. Coll, A. Ben-Ze'ev, R.M. Ezzell, J.L. Rodríguez Fernández, H. Baribault, R.G. Oshima and E.D. Adamson: Proc. Natl. Acad. Sci. USA **92** (1995) 9161–9165.
26) J.D. Humphries, P. Wang, C. Streuli, B. Geiger, M.J. Humphries and C. Ballestrem: J. Cell Biol. **179** (2007) 1043–1057.